Biosensors and Bioelectronics 146 (2019) 111750

Contents lists available at ScienceDirect

Biosensors and Bioelectronics

journal homepage: http://www.elsevier.com/locate/bios

Modulated light-activated electrochemistry at silicon functionalized with metal-organic frameworks towards addressable DNA chips

Jian Wang [a], Zhao Yang [a], Wei Chen [a], Liping Du [a], Bo Jiao [b], Steffi Krause [c], Ping Wang [d], Qiuping Wei [e], De-Wen Zhang [a,*], Chunsheng Wu [a,**]

[a] Institute of Medical Engineering, School of Basic Medical Sciences, Health Science Center, Xi'an Jiaotong University, Xi'an, 710061, China
[b] School of Electronic and Information Engineering, Department of Biophysics, Xi'an Jiaotong University, Xi'an, 10049, China
[c] School of Engineering and Materials Science, Queen Mary University of London, Mile End Road, London, E1 4NS, UK
[d] Biosensor National Special Laboratory, Key Laboratory for Biomedical Engineering of Ministry of Education, Department of Biomedical Engineering, Zhejiang University, Hangzhou, 310027, China
[e] State Key Laboratory of Powder Metallurgy, School of Materials Science and Engineering, Central South University, Changsha, 410083, China

ARTICLE INFO

Keywords:
Light-activated electrochemistry
Light-addressable potentiometric sensor
Metal-organic framework
DNA chip
Photocurrent

ABSTRACT

Modulated light-activated electrochemistry (MLAE) at semiconductor/liquid interfaces derived from light-addressable potentiometric sensor (LAPS) and light-activated electrochemistry (LAE) for addressable photoelectrochemical sensing has been proposed as a new sensor platform. In this system, a bias voltage is applied to create a depletion layer at the silicon/electrolyte interface. Meanwhile, intensity-modulated light illuminates the movable electrode to generate electron/hole pairs and causes a detectable local AC photocurrent. The AC measurement showed a higher signal-to-noise ratio (SNR) of photocurrents compared to the traditional DC response, while a steeper photocurrent-voltage (*I-V*) curve than that of LAPS with an insulating layer was obtained. Furthermore, to stabilize and functionalize the silicon substrate, metal-organic framework (MOF) nanoparticles were grown in-situ on the silicon electrode. The successful modification was validated by X-ray diffraction (XRD) and scanning electron microscopy (SEM). The AC photocurrent increased as a result of the adsorption of negatively charged DNA, which contributed to the enhancement of the cathodic reduction process at the semiconductor electrodes, indicating a different response mechanism of MLAE from LAPS. The results obtained demonstrate the potential of MOF functionalized MLAE as a robust platform for light-addressable DNA chips with high sensitivity and specificity.

1. Introduction

Electrochemical measurements with spatial resolution are essential and important for high-throughput analysis and the investigation of heterogeneous processes. Microelectrode arrays (MEAs) (Obien et al., 2015; Spira and Hai, 2013) and probe-type electrodes (Macazo and White, 2016; Perry et al., 2017; Polcari et al., 2016; Takahashi et al., 2012) have been proposed to achieve spatial discrimination of various analytes. MEAs require a separate sensing electrode with connecting wire for every separate spatial area, multistep fabrication processes and, hence, significant production costs. The geometrical restrictions limit the achievable density of effective working sites on the device. Probe-type electrodes, such as scanning electrochemical microscopy (SECM) (Polcari et al., 2016; Takahashi et al., 2012) and scanning ion conductance microscopy (SICM) (Macazo and White, 2016; Perry et al., 2017), employ an ultramicroelectrode or nanoelectrode tip to scan in close proximity to a surface to record electrochemical information as a function of spatial location, but the tip displacement in solution may cause convective disruption of the measurement, and scanning probe techniques are inherently slow (Licht et al., 1996).

As a probe-less method, light-addressable potentiometric sensors (LAPSs) have been extensively employed for spatially resolved biological investigations (Hafeman et al., 1988; Wang et al., 2018; Yoshinobu et al. 2015, 2017). Based on an electrolyte-insulator-semiconductor (EIS) field-effect structure, a bias voltage is applied to create a depletion layer at the semiconductor/insulator interface. Meanwhile, an

* Corresponding author.
** Corresponding author.
E-mail addresses: zhangdewen@xjtu.edu.cn (D.-W. Zhang), wuchunsheng@xjtu.edu.cn (C. Wu).

https://doi.org/10.1016/j.bios.2019.111750
Received 15 June 2019; Received in revised form 28 August 2019; Accepted 30 September 2019
Available online 3 October 2019

intensity-modulated light illuminates the substrate to generate a local AC photocurrent. The photocurrent is affected by the electrical potential difference at the solid/liquid interface. For example, the adsorption of charged molecules on a sensor surface can alter the interfacial potential and thereby affect the photocurrent output (Wu et al., 2016). An advantage of LAPS is the use of light induced local photocurrents to achieve spatial confinement without the need of a physical probe. In addition, the construction is simple and inexpensive with a single sensor and fewer electrical contacts compared to the conventional pre-determined array scheme. However, the intrinsic drawback of LAPS is that no DC currents cross the interface, which inhibits the electrochemical reactivity of the interface and therefore the scope of the technology is limited to potentiometric measurements (Poghossian and Schöning, 2014; Wu et al., 2019). Light-addressable electrochemistry or light-activated electrochemistry (LAE) (Choudhury et al., 2017; Seo et al., 2018; Vogel et al., 2019; Yang et al. 2016, 2018), which is based on an electrolyte-semiconductor (ES) structure, overcomes this limitation. Light with constant intensity is used to generate electron-hole pairs in a semiconductor biased towards depletion resulting in a DC photocurrent output. This system allows local faradaic currents to cross the ES interface, which broadens the applications to amperometric detection principles.

Recently, the ES structure has also been demonstrated to be suitable for AC photocurrent measurements with spatial addressability (Tu et al., 2018; Wu et al., 2019; Zhang et al., 2017b). The AC photocurrent consists of both, depletion layer charging current and redox current, which is promising for integrating the merits of both LAPS and LAE. The reported sensors with high resolution are based on metal oxide semiconductors such as ITO (Wu et al., 2019; Zhang et al., 2017b) and ZnO (Tu et al., 2018). Silicon is a preferred semiconductor for the development of photoelectrochemical devices due to its narrow band gap, high charge carrier mobility, abundance and well-established fabrication methods in the semiconductor industry. However, the electrochemistry of bare silicon has proven to be very challenging as it is not stable in aqueous media. In DC photocurrent measurement systems, silicon substrates are usually protected with self-assembled organic monolayers (Choudhury et al., 2017; Yang et al. 2016, 2018).

In this study, we investigate the possibility of stable nanoparticle modified silicon as the electrode for spatially resolved AC photocurrent measurements. To stabilize and functionalize the electrode, metal-organic frameworks (MOFs), which are constructed by metal ions/clusters and organic bridging ligands, were prepared on the silicon surface. Due to their prominent properties of flexible porosity, large surface area and facilely tailorable functionality, MOFs have been widely applied as a robust platform for surface immobilization of biosensing elements in the construction of electrochemical biosensors (Ma et al., 2013; Meng et al. 2017, 2018; Zhang et al., 2017a). For instance, they have been used as a matrix for enzyme immobilization on electrodes for highly sensitive electrochemical enzymatic detection (Ma et al., 2013; Zhang et al., 2017a). MOF-based electrochemical sensors for the detection of DNA sequences are very rare thus far (Campbell and Dincă, 2017). Herein, we report modulated light-activated electrochemistry (MLAE) on the basis of MOF nanoparticle modified silicon electrodes for multi-spot label-free DNA sensing. The simple and low-cost device uses intensity-modulated light to irradiate a movable electrolyte-silicon structure to generate local AC photocurrents. The photocurrent was monitored using a lock-in amplifier. UIO-66-NH_2, which is a class of MOFs made of zirconium ions and terephthalate ligands, was deposited on silicon in-situ as the immobilization and sensing matrix for DNA sequences. It will be shown that the proposed system has high specificity and sensitivity for addressable DNA detection on a chip, which opens the door to the application of MOF functionalized silicon-based photoelectrochemical devices in spatially resolved (bio)chemical sensing.

2. Experimental

2.1. Materials

Double polished silicon (100) (boron doped, 1–10 Ω cm, 475 μm) wafers were purchased from Tianjing Yucai optic technology CO, China. All chemicals used for MOF synthesis were obtained commercially from Aladdin Reagents. Bovine serum albumin (BSA) and sodium dodecyl sulfate (SDS) were purchased from Sigma. All solutions were prepared using ultrapure water (18.2 MΩ cm). The sequences of a 25-mer probe, target and mismatched ssDNA molecules used in this study were purchased from Takara (Japan). The probe ssDNA was dissolved in pure water, while the cDNA and nDNA for hybridization were dissolved in 10 mM phosphate buffer with 100 mM NaCl. The sequences are as follows: Probe ssDNA: 5′-GCAGT TGATC CTTTG GATAC CCTGG-3′, or 5′-FITC- GCAGT TGATC CTTTG GATAC CCTGG-3’; target complementary DNA (cDNA): 5′-CCAGG GTATC CAAAG GATCA ACTGC-3′’, or 5′- Texas Red- CCAGG GTATC CAAAG GATCA ACTGC-3; non-complementary DNA (nDNA): 5′-CTCAG CCCTC TTCAA AAACT TCTCC A-3′’, or 5′-Texas Red- CTCAG CCCTC TTCAA AAACT TCTCC A-3.

2.2. Silicon electrode preparation and modification

Double polished p-silicon (100) was used as the electrode. To obtain an ohmic contact, 30 nm Cr and 150 nm Au were thermally evaporated onto the rear side of silicon and subsequently heated to 300 °C for 5 min. Then the wafer was cut into 1.5 cm × 1.5 cm pieces and cleaned in an ultrasonic bath with acetone, isopropyl alcohol, and ultrapure (Milli-Q) water before use.

Nano UIO-66-NH_2 was synthesized according to the published procedure (Wang et al., 2017). First, 108 mg (0.3 mmol) amino-terephthalic acid and 60 μL triethylamine were dissolved in 10 mL dimethylformamide (DMF), while 113.6 mg (0.3 mmol) $ZrCl_4$ and 2.8 mL acetic acid were dissolved in 10 mL DMF, respectively. Then the two solutions were mixed and stirred at room temperature for 1 h. Finally, the mixed solution was transferred into a Teflon reactor chamber with the cleaned silicon substrate and kept in a 120 °C oven for 24 h. The silicon substrate modified with UIO-66-NH_2 was washed consecutively with copious amounts of DMF, methanol and water. A scanning electron microscope (SEM, TESCAN, MALA3 LMH) and X-ray diffraction (XRD, Bruker, D8 ADVANCE) were used to characterize the prepared nanoparticles.

2.3. DNA immobilization and hybridization

For probe DNA immobilization, 4 spots on one MOF-Si substrate were incubated with 5 μL of 5 μM, 2 μM, 0.5 μM and 0.1 μM probe ssDNA solutions for 30 min at room temperature. Then the sensor surface was washed 3 times with pure water to remove any non-attached molecules. Before the detection of target DNA, the sensor substrate was incubated in a solution of 1% BSA +0.05% SDS for 2 h at room temperature to prevent non-specific binding. Then the BSA-blocked sensor spots were exposed to 5 μL hybridization solutions containing different concentrations of target cDNA (from 0.2 nM to 2 μM) or 2 μM mismatched ssDNA, respectively, for 30 min at room temperature, followed by washing 3 times with pure water. The incubation processes were all performed in a closed Petri dish with a moistened tissue to prevent the small amount of DNA solutions from drying.

2.4. DC photocurrent measurements

A laser (Thorlabs, λ = 405 nm, max. 20 mW) controlled by LDC202C controller (Thorlabs) was used as the light source for activation. DC photocurrents were detected by a potentiostat analyser (Zennium, Zahner Elektrik, Germany). Linear sweep voltammetry (LSV) was carried out in 10 mM pH 7.4 phosphate buffered saline (PBS, 137 mM NaCl, 2.7 mM KCl, 10 mM Na_2HPO_4, 2 mM KH_2PO_4) with a scan rate of 5 mV/

s. Chronoamperometry was carried out in 10 mM pH 7.4 PBS with the laser chopped at 0.1 Hz. For all measurements, a platinum electrode and an Ag/AgCl electrode were used as the counter and reference electrodes, respectively.

2.5. MLAE measurements

The MLAE setup is shown in Fig. 1. A laser diode module (Thorlabs, $\lambda = 405$ nm, max. 20 mW) controlled by LDC202C controller (Thorlabs) was used for the generation of charge carriers. The diameter of the laser beam illuminated on the sensor surface is around 0.7 mm. The testing chamber was designed to have 6 holes with a diameter of 1 mm and 1.5 mm spacing at the bottom, resulting in 6 measurement spots on one electrode. These spots can be addressed by moving the silicon electrode mounted onto the PILine® XY stage (U723.25, Physik Instrumente (PI Shanghai) Co., Ltd.) with 10 nm sensor resolution and 0.1 μm minimum incremental motion. Since the diameter of the laser spot is smaller than that of the sensing spots, by adjusting the positioning stages, the laser beam can just illuminate one of the sensing wells. The AC photocurrent was measured using a SR830 lock-in amplifier. A platinum electrode and an Ag/AgCl electrode moved with the working electrode were used as the counter and reference electrodes, respectively. For pH sensitivity measurements a range of 10 mM phosphate buffer (pH 4–9) with 0.1 M NaCl were used. For DNA sensing, 10 mM pH 7.4 PBS was adopted. The control program used for the measurements was written in LabView.

3. Results and discussion

3.1. Photoelectrochemical responses of a p-type silicon electrode

To investigate the effect of the modulation frequency on the AC photocurrent, the photocurrent and background current in the dark at -0.6V, were measured from 5 to 10,000 Hz in pH 7.4 PBS. As shown in Fig. 2a, the AC photocurrent increased with the frequency, while the dark current stayed constant at instrumental noise level. A high signal-to-noise ratio (SNR) of the photocurrent can be obtained with a frequency higher than 100 Hz. The result differs from the ITO-based electrode with an optimized frequency of 10 Hz (Wu et al., 2019; Zhang et al., 2017b), indicating that silicon would be a more promising electrode material for high speed measurements. 1 kHz was chosen as the measurement frequency in this work. Fig. 2b–c shows the AC at 1 kHz and DC *I-V* curves of silicon in pH 7.4 PBS. The shape of the AC *I-V* curve for MLAE (Fig. 2b) was analogous to the typical *I-V* curve for a p-doped**type** LAPS, which consists of three regions of accumulation, depletion and inversion (Wagner and Schöning, 2007). The AC dark current was significantly smaller than the photocurrent (Fig. 2b), while the DC background current was comparable to the photocurrent for cathodic potentials up to -0.6 V (Fig. 2c), revealing a much higher SNR of MLAE for photoelectrochemical measurements.

A comparison of AC *I-V* curves of silicon with and without an insulator is presented in Fig. 3a. Due to the absence of insulator, the *I-V* curve of the bare silicon substrate is steeper and displays a greater photocurrent resulting in a higher sensitivity of photocurrent measurements. Fig. 3b–c shows pH responses of the bare silicon in a series of pH PBS (10 mM, 0.1 M NaCl, pH 4–9) using MLAE and the corresponding calibration plot. An average pH sensitivity of about 47 mV/pH was obtained, which was higher than that of the traditional LAPS insulated with 70 nm SiO_2 (31 mV/pH, see Supporting Information, Fig. S1). Referring to our previous report (Zhang et al., 2017b), the sensitivity is due to the pH dependent kinetics of the faradaic process on the silicon surface. Since the silicon is p-type, the current is cathodic and it can be attributed to the reduction of H^+.

3.2. Surface modification with MOF nanoparticles

MOF has been shown to be a great platform for the adsorption of DNA (Liu et al., 2012; Tian et al., 2015; Zhang et al., 2014; Zhao et al., 2016). UIO-66-NH_2 was chosen to decorate silicon as it is highly stable in water and biocompatible in biological system compared to other kinds of MOF materials (Ruyra et al., 2015). In addition, the electrostatic attractions such as π-π stacking or hydrogen bond interactions between UIO-66-NH_2 and the aromatic nucleotide bases of DNA facilitate efficient and high-affinity binding (Wang et al., 2017). The successful preparation of MOF nanoparticles on silicon was confirmed in SEM images (Fig. 4a–b). It was shown the nanoparticles with an average diameter of 150 ± 20 nm were uniformly distributed over the silicon surface without aggregation. The particles showed regular octahedron structure, which was the typical shape of UIO-66-NH_2 based MOF. The percentage surface coverage of MOF nanoparticles on silicon was estimated using ImageJ. An average surface coverage of $70\% \pm 3.2\%$ (SD) with 6 batches of samples was obtained, indicating a reliable immobilization protocol. Typical X-ray diffraction (XRD) measurements were used to establish the crystal phase of the UIO-66-NH_2. As shown in Fig. 4c, all the diffraction peaks of the MOF powder corresponded well to the simulated pattern derived from the single-crystal X-ray diffraction data. As shown in Fig. 4c, the XRD pattern collected for UIO-66-NH_2 grown on silicon (trace B) agreed well with the powder XRD pattern (trace A) in terms of some main peaks, demonstrating the formation of pure-phase UIO-66-NH_2.

As there is unlikely to be any chemical reaction between UIO-66-NH_2 and silicon, MOF nanoparticles are physically absorbed on the silicon surface. Fig. S2a shows the effect of MOF adsorption on the AC

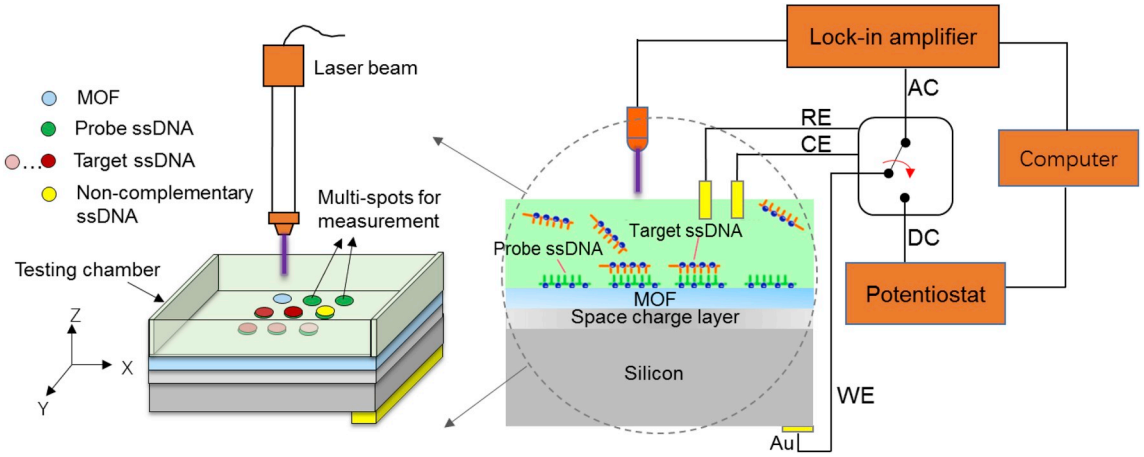

Fig. 1. Experimental scheme of silicon-based MLAE.

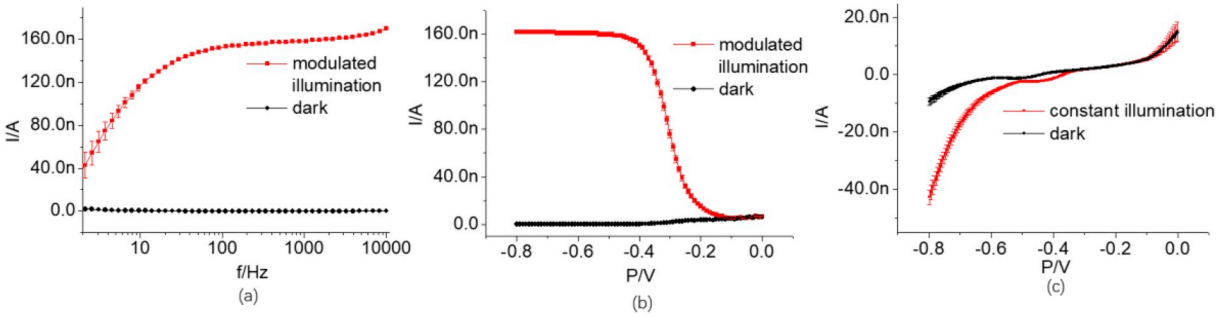

Fig. 2. (a) The frequency dependence of the AC photocurrent (red) and background AC current in the dark (black) biased at -0.6 V. (b) AC current-voltage (*I-V*) curves measured with lock-in amplifier (1 kHz) and (c) DC *I-V* curves measured with a potentiostat with a 405 nm laser (red) and dark (black). Each data point is an average of the 6 measurements on 6 sensing spots on one electrode and is presented as mean ± SD. (For interpretation of the references to colour in this figure legend, the reader is referred to the Web version of this article.)

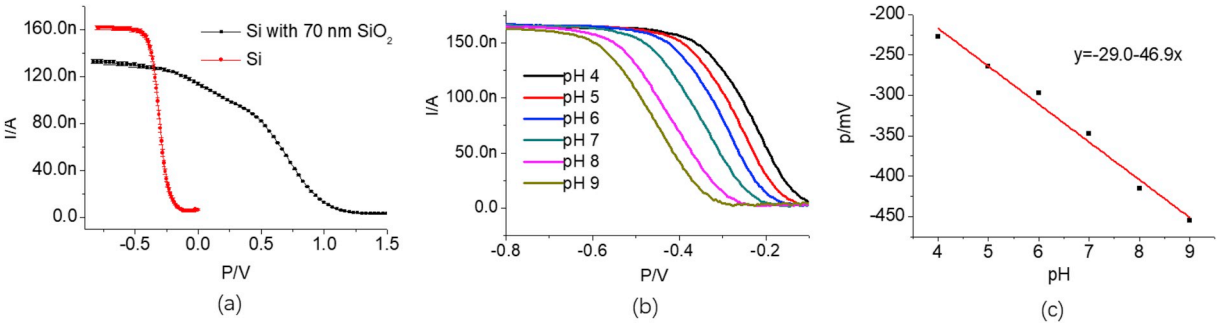

Fig. 3. (a) AC *I-V* curves of p-silicon substrates with and without insulator measured with the same laser intensity. Each data point is an average of the 6 measurements on 6 sensing spots on one electrode and is presented as mean ± SD. (b) AC *I-V* curves at different pH values and (c) corresponding calibration plot.

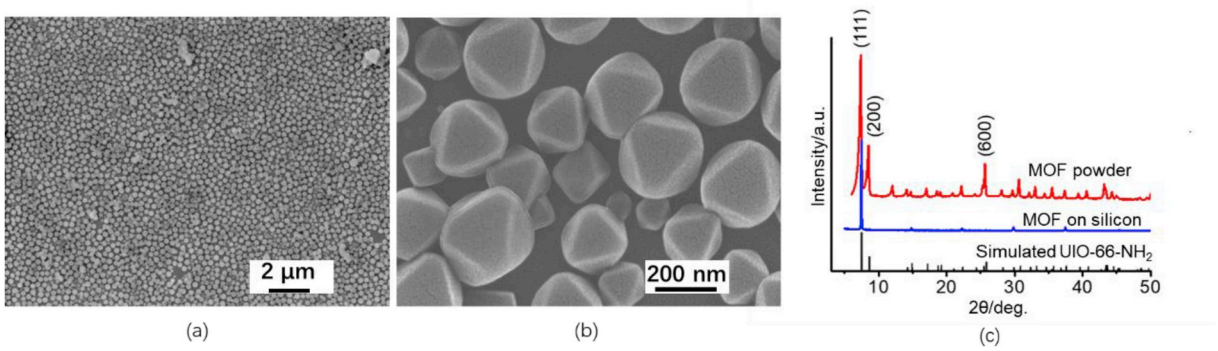

Fig. 4. Typical SEM top view of UIO-66-NH_2 nanoparticles grown on p-Si (100) surface (a) overview and (b) zoomed images. (c) XRD patterns for simulated UIO-66-NH_2, UIO-66-NH_2 powder and UIO-66-NH_2 grown on bare silicon. (For interpretation of the references to colour in this figure legend, the reader is referred to the Web version of this article.)

photocurrent output of the sensor platform. After the modification of silicon with MOF, the *I-V* curve measured with laser illumination shifted and the photocurrent decreased significantly, which may be attributed to the positive charge and poor conductivity of UIO-66-NH_2 MOF. On the other hand, the dark current stayed significantly smaller and showed almost no change due to MOF immobilization. The stability of the MOF-modified silicon electrode (MOF-Si) was evaluated using AC *I-V* measurements. Fig. S2b shows potential shifts of *I-V* curves in PBS for the MOF-Si and Si electrodes measured over 5 h. One can see that there was only small perturbation of *I-V* curves for the MOF-Si sample, while obvious shifts were observed for the bare Si electrode, indicating a passivation effect resulting from the modification with MOF nanoparticles.

3.3. Probe ssDNA adsorption on MOF-Si

MOF-Si and bare silicon substrates were incubated respectively with a drop (5 μL) of 2 μM probe single-stranded (ss)DNA labelled with FITC. The incubation process was performed in a closed Petri dish with a moistened tissue to prevent the small amount of DNA solutions from drying. Then the substrates were washed 3 times with pure water to remove any non-attached DNA molecules. As displayed in Fig. 5a, the MOF-Si surface exhibited strong fluorescence emission with the presence of the probe FITC-ssDNA, while bare silicon showed insignificant fluorescence (data not shown), demonstrating the feasibility of amine-functionalized MOF as a great platform for DNA adsorption. The strong binding is probably due to the electrostatic attraction as DNA carries negative charge while UIO-66-NH_2 showed a slightly positive zeta potential (~3.4 mV). After DNA adsorption, the zeta potential

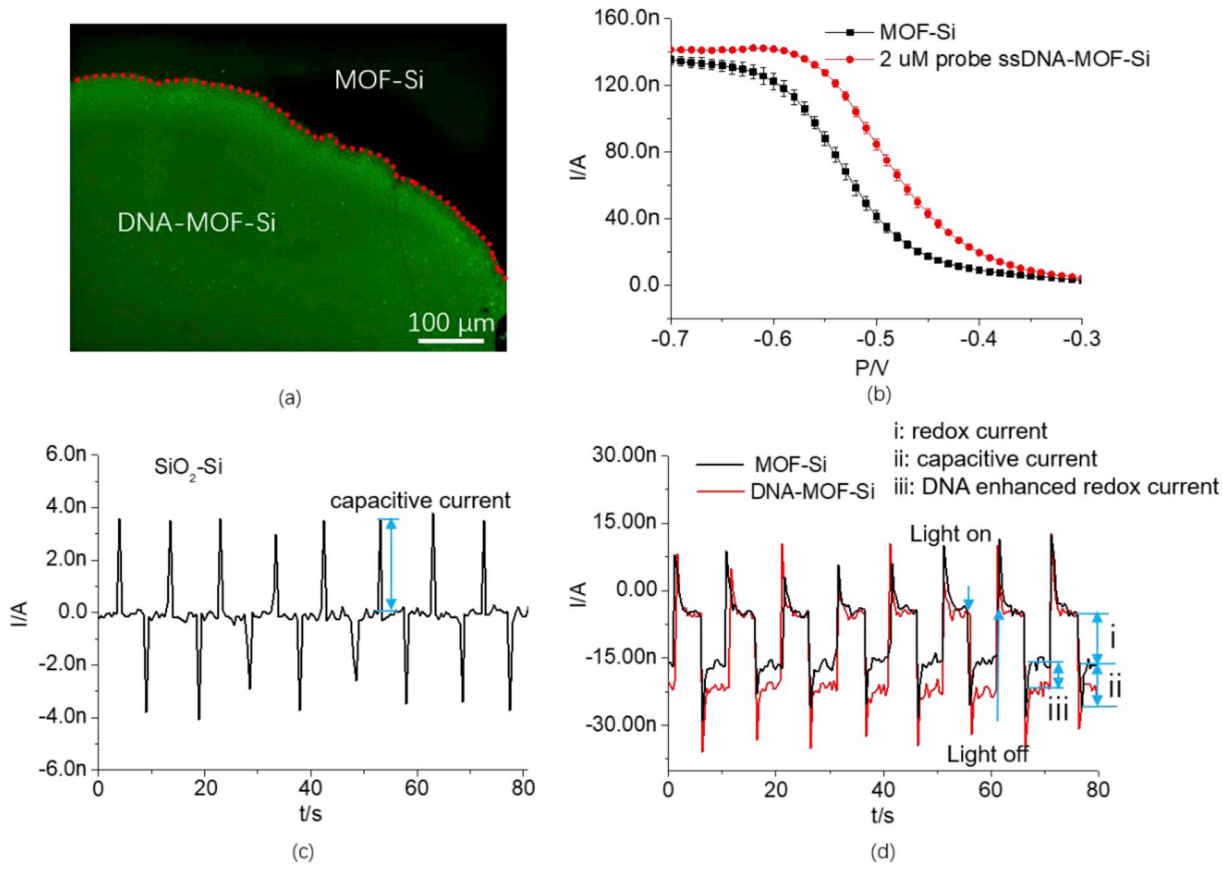

Fig. 5. (a) Fluorescence image taken from MOF-Si surface after incubated with a drop of 2 μM FITC-labelled probe ssDNA solution; (b) AC *I-V* curves measured before and after the probe ssDNA adsorption. Each data point is an average of the 6 measurements and is presented as mean ± SD. *I-t* curves measure with potentiostat at -0.6 V with a chopped laser illumination of 0.1 Hz on (c) SiO_2-Si and on (d) MOF-Si without (black) and with (red) probe DNA adsorption. (For interpretation of the references to colour in this figure legend, the reader is referred to the Web version of this article.)

changed to -6.7 mV, which was consistent to the result shown in (Wang et al., 2017). Moreover, the addition of acetic acid introduces additional defects in UIO-66-NH_2, which are also beneficial for DNA binding (Wang et al., 2017).

To investigate the effect of the probe ssDNA concentration on the MLAE signal, the probe molecules were immobilized from solutions of 0.1 μM, 0.5 μM, 2 μM and 5 μM ssDNA. The *I-V* curve shifted from 20 mV to 46 mV with increasing ssDNA concentration from 0.1 μM to 2 μM and stayed almost stable beyond 2 μM (Fig. S3a). As the optimized result, 2 μM probe ssDNA was chosen for immobilization in our next experiments. Again, there is no effect of DNA adsorption on the dark current (see Fig. S2a). Fig. 5b shows *I-V* curves before and after probe ssDNA adsorption measured with 405 nm laser. A positive shift (or an increase of photocurrent) was observed, which was opposite to that of conventional LAPS (Wang et al., 2015; Wu et al., 2015). The main difference in the two techniques is the absence of an insulator layer in MLAE, resulting in the generation of a redox current on the semiconductor electrode (Wu et al., 2019). Fig. 5c and d illustrate the photocurrent changes with chopped light (0.1 Hz) at -0.6 V measured with a potentiostat. For SiO_2-Si, only capacitive current spikes were observed due to the charge and discharge of the depletion layer of Si with the light switched on and off (Fig. 5c). On the other hand, the MOF-Si electrode showed a combination of capacitive current and photocatalytic redox current (Fig. 5d in black). Since DNA is negatively charged, it would increase the surface concentrations of hydrogen ions at the electrode and accelerate the cathodic reduction process, thus resulting in a higher redox current compared to the sensor surface without DNA (see Fig. 5d in red). This indicates that the sensitivity of MLAE can extend to charges in the diffusion layer (~μm), which is no longer limited to Debye length (~0.7 nm in the PBS buffer) induced by counter-ion screening effects as that of traditional field-effect devices.

3.4. Target ssDNA detection using MLAE

The non-specific adsorption of target DNA on probe ssDNA-MOF-Si was investigated. Fig. S3b shows the *I-V* curves before and after hybridization with 2 μM complementary and non-complementary DNA (cDNA, nDNA). The hybridization with cDNA (2 μM) results in a greater positive shift of the *I-V* curves or a higher photocurrent signal at the depleted semiconductor. As mentioned above, this increase in photocurrent is attributed to the electrostatic attraction of hydrogen ions to the negatively charged cDNA. For the case of nDNA, a smaller but significant increase in photocurrent was also observed (see Fig. S3b), indicating the non-specific adsorption of target DNA on the sensor surface.

As a good antifouling agent, BSA was used to prevent non-specific binding of target DNA on the sensor interface. Photocurrent measurements showed that BSA adsorption did not affect cDNA binding and sensing, while the non-specific binding of nDNA was significantly reduced (Fig. 6a). This is also demonstrated through fluorescent images of DNA with and without BSA incubation (Fig. S4).

The BSA-blocked 6 spots on one semiconductor electrode were exposed to 5 μL hybridization solutions with different concentrations of target cDNA (0.2 nM, 2 nM, 20 nM, 200 nM, 2 μM) or 2 μM mismatched ssDNA, respectively, for 30 min at room temperature. Fig. 6b presents the dependence of the hybridization signal of MOF-Si on the target cDNA concentration ranging from 0.2 nM to 2 μM on one chip. The hybridization signal increases with increasing target cDNA concentration and

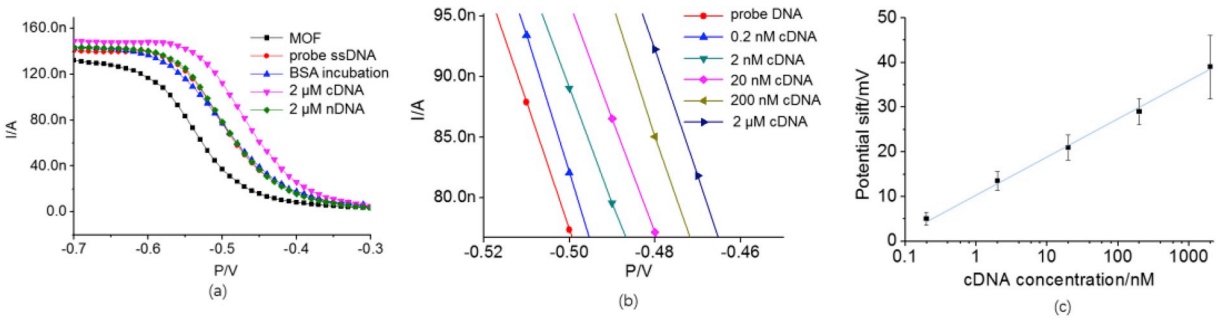

Fig. 6. AC *I-V* curves recorded (a) from a single channel before and after ssDNA adsorption, after incubation with BSA, after non-specific adsorption of nDNA, and after hybridization with cDNA; (b) from five channels modified with 2 μM probe ssDNA when exposed to serial concentrations of concentrations of cDNA (0.2 nM, 2 nM, 20 nM, 200 nM and 2 μM, respectively) and (c) the corresponding statistical results of the hybridization signals of the MLAE in response to different cDNA concentrations. The mean and stand error of the mean of three experiments are shown.

achieves a value of 34 mV at 2 μM cDNA. At a very low cDNA concentration of 0.2 nM, a detectable hybridization signal of 4 mV was registered, which is similar to the shift resulting from nDNA adsorption with a much higher concentration (2 μM *vs.* 0.2 nM). These results indicate a good specificity and sensitivity of the developed technique allowing the successful discrimination between target DNA analytes with different concentration on one semiconductor electrode. For specific applications, further investigations such as the effect of single mismatched DNA will be required for the exploitation of the new sensor platform.

4. Conclusions

Modulated light-activated electrochemistry (MLAE) based on AC photocurrent measurements at metal-organic frameworks (MOFs) functionalized silicon was developed for addressable DNA detection. The AC measurements showed a higher signal-to-noise ratio (SNR) of photocurrents and a steeper photocurrent-voltage (*I-V*) curve compared to the related techniques of LAE and LAPS. In addition, the proposed system was proven to be a robust platform for spatially resolved detection of DNA molecules. Metal-organic framework (MOF) nanoparticles (UIO-66-NH_2) were deposited on silicon electrodes for probe DNA immobilization. The *I-V* results showed that the hybridization signal of complementary DNA (cDNA) increases from 4 mV to 34 mV with increasing the concentration of cDNA from 0.2 nM to 2 μM on one chip. In contrast, a small signal of 5 mV was recorded for the non-complementary DNA adsorption (5 μM). This example demonstrated the potential of MOF functionalized MLAE as a simple and low-cost platform for multi-spot and label-free bio(chemical) molecule detection with good sensitivity and specificity.

Declaration of competing interest

The authors declare that they have no known competing financial interests or personal relationships that could have appeared to influence the work reported in this paper.

CRediT authorship contribution statement

Jian Wang: Data curation, Formal analysis, Methodology, Writing - original draft, Writing - review & editing. **Zhao Yang:** Data curation, Formal analysis, Resources. **Wei Chen:** Methodology, Software, Conceptualization. **Liping Du:** Investigation, Methodology, Validation. **Bo Jiao:** Investigation, Resources. **Steffi Krause:** Conceptualization, Writing - review & editing. **Ping Wang:** Funding acquisition, Project administration. **Qiuping Wei:** Investigation, Methodology. **De-Wen Zhang:** Conceptualization, Formal analysis, Project administration, Supervision, Writing - review & editing. **Chunsheng Wu:** Resources, Funding acquisition, Supervision, Writing - review & editing.

Acknowledgments

This work was supported by the National Natural Science Foundation of China (Grant No. 31800827, 31661143030, 51861145307), Shanxi Provincial Natural Science Foundation (Grant No. 2018JQ8058), the Doctoral Fund of Education Ministry of China (Grant No. 2017M613146), and the Fundamental Research Funds for the Central Universities.

Appendix A. Supplementary data

Supplementary data to this article can be found online at https://doi.org/10.1016/j.bios.2019.111750.

References

Campbell, M., Dincă, M., 2017. Metal–organic frameworks as active materials in electronic sensor devices. Sensors 17 (5), 1108.
Choudhury, M.H., Ciampi, S., Lu, X., Kashi, M.B., Zhao, C., Gooding, J.J., 2017. Spatially confined electrochemical activity at a non-patterned semiconductor electrode. Electrochim. Acta 242, 240–246.
Hafeman, D., Parce, J., McConnell, H., 1988. Light-addressable potentiometric sensor for biochemical systems. Science 240 (4856), 1182–1185.
Licht, S., Myung, N., Sun, Y., 1996. A light addressable photoelectrochemical cyanide sensor. Anal. Chem. 68 (6), 954–959.
Liu, S., Wang, L., Tian, J., Luo, Y., Chang, G., Asiri, A.M., Al-Youbi, A.O., Sun, X., 2012. Application of zeolitic imidazolate framework-8 nanoparticles for the fluorescence-enhanced detection of nucleic acids. ChemPlusChem 77 (1), 23–26.
Ma, W., Jiang, Q., Yu, P., Yang, L., Mao, L., 2013. Zeolitic imidazolate framework-based electrochemical biosensor for in vivo electrochemical measurements. Anal. Chem. 85 (15), 7550–7557.
Macazo, F.C., White, R.J., 2016. Bioinspired protein channel-based scanning ion conductance microscopy (Bio-SICM) for simultaneous conductance and specific molecular imaging. J. Am. Chem. Soc. 138 (8), 2793–2801.
Meng, W., Wen, Y., Dai, L., He, Z., Wang, L., 2018. A novel electrochemical sensor for glucose detection based on Ag@ZIF-67 nanocomposite. Sens. Actuators B Chem. 260, 852–860.
Meng, W., Xu, S., Dai, L., Li, Y., Zhu, J., Wang, L., 2017. An enhanced sensitivity towards H2O2 reduction based on a novel Cu metal–organic framework and acetylene black modified electrode. Electrochim. Acta 230, 324–332.
Obien, M.E.J., Deligkaris, K., Bullmann, T., Bakkum, D.J., Frey, U., 2015. Revealing neuronal function through microelectrode array recordings. Front. Neurosci. 8, 423-423.
Perry, D., Page, A., Chen, B., Frenguelli, B.G., Unwin, P.R., 2017. Differential-concentration scanning ion conductance microscopy. Anal. Chem. 89 (22), 12458–12465.
Poghossian, A., Schöning, M.J., 2014. Label-free sensing of biomolecules with field-effect devices for clinical applications. Electroanalysis 26 (6), 1197–1213.
Polcari, D., Dauphin-Ducharme, P., Mauzeroll, J., 2016. Scanning electrochemical microscopy: a comprehensive review of experimental parameters from 1989 to 2015. Chem. Rev. 116 (22), 13234–13278.
Ruyra, À., Yazdi, A., Espín, J., Carné-Sánchez, A., Roher, N., Lorenzo, J., Imaz, I., Maspoch, D., 2015. Synthesis, culture medium stability, and in vitro and in vivo Zebrafish embryo toxicity of metal–organic framework nanoparticles. Chem. Eur J. 21 (6), 2508–2518.
Seo, D., Lim, S.Y., Lee, J., Yun, J., Chung, T.D., 2018. Robust and high spatial resolution light addressable electrochemistry using hematite (α-Fe2O3) photoanodes. ACS Appl. Mater. Interfaces 10 (39), 33662–33668.

Spira, M.E., Hai, A., 2013. Multi-electrode array technologies for neuroscience and cardiology. Nat. Nanotechnol. 8, 83.
Takahashi, Y., Shevchuk, A.I., Novak, P., Babakinejad, B., Macpherson, J., Unwin, P.R., Shiku, H., Gorelik, J., Klenerman, D., Korchev, Y.E., Matsue, T., 2012. Topographical and electrochemical nanoscale imaging of living cells using voltage-switching mode scanning electrochemical microscopy. Proc. Natl. Acad. Sci. U.S.A. 109 (29), 11540–11545.
Tian, J., Liu, Q., Shi, J., Hu, J., Asiri, A.M., Sun, X., He, Y., 2015. Rapid, sensitive, and selective fluorescent DNA detection using iron-based metal–organic framework nanorods: synergies of the metal center and organic linker. Biosens. Bioelectron. 71, 1–6.
Tu, Y., Ahmad, N., Briscoe, J., Zhang, D.-W., Krause, S., 2018. Light-addressable potentiometric sensors using ZnO nanorods as the sensor substrate for bioanalytical applications. Anal. Chem. 90 (14), 8708–8715.
Vogel, Y.B., Gooding, J.J., Ciampi, S., 2019. Light-addressable electrochemistry at semiconductor electrodes: redox imaging, mask-free lithography and spatially resolved chemical and biological sensing. Chem. Soc. Rev. 48 (14), 3723–3739.
Wagner, T., Schöning, M.J., 2007. Chapter 5 Light-addressable potentiometric sensors (LAPS): recent trends and applications. In: Alegret, S., Merkoçi, A. (Eds.), Comprehensive Analytical Chemistry. Elsevier, pp. 87–128.
Wang, J., Du, L., Krause, S., Wu, C., Wang, P., 2018. Surface modification and construction of LAPS towards biosensing applications. Sens. Actuators B Chem. 265, 161–173.
Wang, J., Zhou, Y., Watkinson, M., Gautrot, J., Krause, S., 2015. High-sensitivity light-addressable potentiometric sensors using silicon on sapphire functionalized with self-assembled organic monolayers. Sens. Actuators B Chem. 209, 230–236.
Wang, Z., Fu, Y., Kang, Z., Liu, X., Chen, N., Wang, Q., Tu, Y., Wang, L., Song, S., Ling, D., Song, H., Kong, X., Fan, C., 2017. Organelle-specific triggered release of immunostimulatory oligonucleotides from intrinsically coordinated DNA–metal–organic frameworks with soluble exoskeleton. J. Am. Chem. Soc. 139 (44), 15784–15791.
Wu, C., Bronder, T., Poghossian, A., Werner, C.F., Schöning, M.J., 2015. Label-free detection of DNA using a light-addressable potentiometric sensor modified with a positively charged polyelectrolyte layer. Nanoscale 7 (14), 6143–6150.
Wu, C., Poghossian, A., Bronder, T.S., Schöning, M.J., 2016. Sensing of double-stranded DNA molecules by their intrinsic molecular charge using the light-addressable potentiometric sensor. Sens. Actuators B Chem. 229, 506–512.
Wu, F., Zhou, B., Wang, J., Zhong, M., Das, A., Watkinson, M., Hing, K., Zhang, D.-W., Krause, S., 2019. Photoelectrochemical imaging system for the mapping of cell surface charges. Anal. Chem. 91, 5896–5903.
Yang, Y., Ciampi, S., Zhu, Y., Gooding, J.J., 2016. Light-activated electrochemistry for the two-dimensional interrogation of electroactive regions on a monolithic surface with dramatically improved spatial resolution. J. Phys. Chem. C 120 (24), 13032–13038.
Yang, Y., Cuartero, M., Gonçales, V.R., Gooding, J.J., Bakker, E., 2018. Light-addressable ion sensing for real-time monitoring of extracellular potassium. Angew. Chem. Int. Ed. 57 (51), 16801–16805.
Yoshinobu, T., Miyamoto, K.-i., Wagner, T., Schöning, M.J., 2015. Recent developments of chemical imaging sensor systems based on the principle of the light-addressable potentiometric sensor. Sens. Actuators B Chem. 207, 926–932.
Yoshinobu, T., Miyamoto, K.-i., Werner, C.F., Poghossian, A., Wagner, T., Schöning, M.J., 2017. Light-addressable potentiometric sensors for quantitative spatial imaging of chemical species. Annu. Rev. Anal. Chem. 10 (0), 225–246.
Zhang, C., Wang, X., Hou, M., Li, X., Wu, X., Ge, J., 2017. Immobilization on metal–organic framework engenders high sensitivity for enzymatic electrochemical detection. ACS Appl. Mater. Interfaces 9 (16), 13831–13836.
Zhang, D.-W., Wu, F., Krause, S., 2017. LAPS and SPIM imaging using ITO-coated glass as the substrate material. Anal. Chem. 89 (15), 8129–8133.
Zhang, H.-T., Zhang, J.-W., Huang, G., Du, Z.-Y., Jiang, H.-L., 2014. An amine-functionalized metal–organic framework as a sensing platform for DNA detection. Chem. Commun. 50 (81), 12069–12072.
Zhao, H.-Q., Qiu, G.-H., Liang, Z., Li, M.-M., Sun, B., Qin, L., Yang, S.-P., Chen, W.-H., Chen, J.-X., 2016. A zinc(II)-based two-dimensional MOF for sensitive and selective sensing of HIV-1 ds-DNA sequences. Anal. Chim. Acta 922, 55–63.